Aging and Lifetime of Power Module Packaging Insulation Due to Partial Discharge Under High d*V*/d*t* Square Wave Voltage and High Temperature

Yi Ding, Yalin Wang, *Member, IEEE*, Meng Chen, *Student Member, IEEE*, Lu Fan, and Yi Yin, *Member, IEEE*

***Abstract*—The application of wide bandgap semiconductors poses challenges to the packaging reliability of power modules under high d*V*/d*t* square wave voltage and high temperatures. The partial discharge (PD) occurring in the encapsulant is one of the main causes resulting in packaging insulation aging and failure. However, limited research focuses on the effects of temperature and square wave parameters on packaging insulation aging principle and the exact mechanisms remain largely unknown. To address that, this article focuses on the aging process of power module packaging insulation due to PD under high d*V*/d*t* square wave and high-temperature coupling stresses. The specially designed down-mixing PD detection system is applied to extract PD signals during aging. The experimental results indicate that the magnitude of PD shows a fluctuating growth trend during aging, and PD activity reaches severest before breakdown. As the temperature rises, the lifetime of the power module packaging insulation decreases, accompanied by an increase in the magnitude and pulse repetition rate of PDs. The longer rise time and lower voltage frequency of the square wave usually lead to longer lifetimes. The effects of temperature, rise time, and voltage frequency on PD behaviors are analyzed based on the discharge mechanism and finite element electric field simulation. Moreover, the total accumulation damage of PD during aging is primarily correlated with temperature, and based on that, the lifetime estimation model of power module packaging insulation considering temperature and PD aging factors is proposed for the first time, which provides the reference for the condition evaluation of the power module.**

***Index Terms*—Aging, high temperature, lifetime, partial discharge, power module, packaging insulation.**

I. Introduction

THE reliability of the power module plays a critical role in power conversion and transmission, which serves as a key factor in the stable operation of the power system. The issues of power module failure due to packaging insulation aging account for a significant proportion [1]. With the application of wide bandgap (WBG) semiconductors, silicon carbide (SiC) for example, the new generation of power chips provides faster switching speeds, higher operation voltages, higher operating temperatures, and smaller size, which poses more challenges to the reliability of the power module packaging insulation at high temperature and high voltage (HV) [2]. In light of this current situation, it is essential to conduct research on the aging and lifetime characteristics of power module packaging under high temperature and high voltage coupling stresses. Existing research on power module aging mainly focuses on the damage of dies and packaging caused by thermal stress and power cycling, such as emitter metallization of the semiconductor die, the increase of on-state voltage drop [3], [4], [5], fatigue, deteriorating the thermal and electrical performance [6], [7], and the bonding wire failures [8], [9], [10].

The semiconductor die of the power module typically operates in switch mode, with either a freewheeling diode connected in reverse parallel across its two terminals or an intrinsic parasitic reverse diode [10]. Therefore, the packaging insulation generally operates under the unipolar square wave voltage. The short switching time and high operation voltage provide high d*V*/d*t* (also known as slew rate, SR) of up to tens or even hundreds of V/ns with the development of WBG semiconductors. Under unipolar high d*V*/d*t* square wave voltage, the energy generation and transfer processes include the local distribution of electrostatic and electromechanical energy, the release of trapped charge energy, energy transfer due to carrier recombination, and the energy release from polarons due to released charges. The various charge-energy interactions of microscopic charges under square wave voltages may damage the molecular structure by generating hot-electron bombardment of molecular chains, transferring energy through recombination luminescence, and mechanical stress cycling. That can lead to the formation of mesoscopic micro defects such as free radicals and low-density regions and with the accumulation of damages, the mesoscopic or micro defects develop into macroscopic cavities/air gaps, which in turn trigger the partial discharge (PD) [11]. The PD occurring in the encapsulant (such as silicone gel or elastomer) is one of the main causes resulting in packaging insulation

Received 3 July 2024; revised 29 October 2024 and 13 January 2025; accepted 24 February 2025. Date of publication 3 March 2025; date of current version 14 April 2025. This work was supported in part by the National Natural Science Foundation of China under Grant 52477149, in part by Young Elite Scientists Sponsorship Program by CAST under Grant 2023QNRC001, and in part by Shanghai Pujiang Program under Grant 22PJ1407800. Recommended for publication by Associate Editor C. DiMarino. *(Corresponding author: Yalin Wang.)*

The authors are with the Department of Electrical Engineering, State key Laboratory of High-Efficiency special cable technology, Shanghai Jiao Tong University, Shanghai 200240, China (e-mail: 2018-ee-dingyi@sjtu.edu.cn; wangyalin2014@sjtu.edu.cn; cm3540@sjtu.edu.cn; fan-lu@sjtu.edu.cn; yiny@sjtu.edu.cn).

Color versions of one or more figures in this article are available at https://doi.org/10.1109/TPEL.2025.3546407.

Digital Object Identifier 10.1109/TPEL.2025.3546407

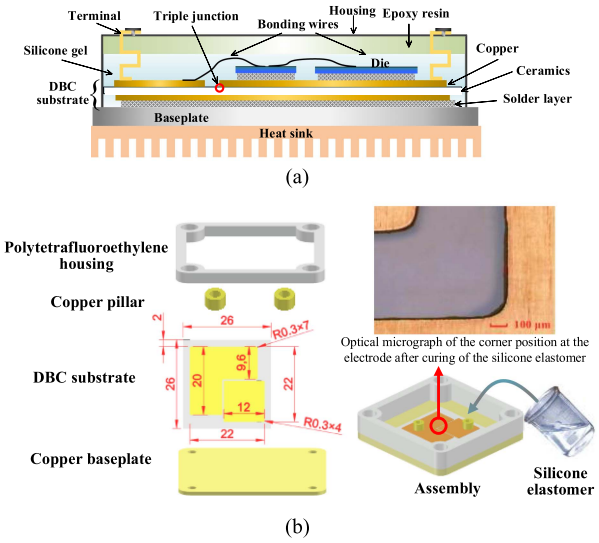

Fig. 1. (a) Components of a typical power module. (b) Components and their assembly of the specimen.

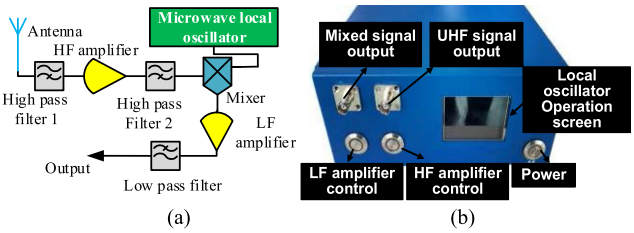

Fig. 2. Circuit diagram (a) and photo (b) of the down-mixing PD detection system.

degradation, aging, and even breakdown. The study on the operating temperature of a SiC-based power module shows that the junction temperature can reach more than 200 °C [1]. High temperatures affect the dielectric properties of insulation materials and PD behaviors, resulting in severe damage and aging of packaging insulation [12], [13], [14], [15], [16]. However, the aging failure of power module packaging insulation caused by PDs, and the PD evolution during the aging process at high temperatures are rarely reported. Studies on electrical trees and PD behaviors during tree growth in silicone gel for power module packaging indicate that higher voltage frequency, shorter voltage rise time, and higher temperature can lead to lower electrical tree inception voltage, longer tree length, and more severe PDs [17], [18], [19], [20], [21], [22]. Although electrical treeing growth can provide references for packaging insulation aging due to PDs, the experimental samples of electrical trees are mostly designed based on the needle-plane structure and differ significantly from the actual electrode shape inside power modules. Therefore, it is inappropriate to analyze the aging of power modules solely based on the electrical treeing growth, and the test sample consistent with the packaging insulation structure and actual operation voltage of the power module should be used for PD aging research.

Characteristics of charge transport, PDs, and lifetime of solid insulation materials under high dV/dt are rarely studied, which differ from those under conventional sinusoidal and dc voltages [23]. Moreover, the rapid electric field change due to the high dV/dt of the square wave causes displacement currents and electromagnetic waves, which severely interfere with PD detection, bringing difficulty in studying PD evolution during the aging process. In our previous work, high-pass filtering and down-mixing techniques are combined to suppress electromagnetic interference (EMI) and effectively extract the discharge signal [2], [23], [24], [25], laying the foundation for investigating the evolution of PDs in the power module packaging insulation during aging in this article.

To address the aging and failure of power module packaging insulation due to PDs, this article focuses on the PD evolution and aging process of power module packaging insulation under high dV/dt square wave and high-temperature coupling stresses, providing the reference for the research on the lifetime and reliability of power modules. The specially designed down-mixing PD detection system is applied to extract and continuously record PD data during aging. The evolution of the magnitude and pulse repetition rate of PDs and the lifetime during aging under different temperatures are investigated first. Subsequently, the effects of square wave rise time and voltage frequency on PD characteristics during aging and lifetime are studied. The effects of temperature, rise time, and voltage frequency on PD evolution are analyzed based on the discharge mechanism and finite element electric field simulation. Moreover, a lifetime model of power module packaging insulation considering the aging effects of high temperature and PD damage accumulation is proposed for the first time based on the analysis of PD evolution.

II. Experiment Setup

A. Specimen Design and Fabrication

The specimen for aging experiments is based on the actual packaging structure of the power module. Fig. 1(a) shows the components and internal structure of a typical power module. The study about electric field based on finite element analysis shows that the triple junction of the encapsulant-copper-ceramics of direct-bonding copper (DBC) substrate edges is usually the high electric field point and PD inception position [26], as marked by the red circle in Fig. 1(a). Based on the components and structures shown in Fig. 1(a), the specimen consists of a DBC substrate, a copper baseplate, two soldered copper pillars, and a polytetrafluoroethylene housing, as shown in Fig. 1(b). The curvature radius of the electrodes of the DBC substrate is 0.3 mm and the distance from the L-shaped electrode to the square electrode is 0.5 mm. The thicknesses of the copper electrodes and the Al_2O_3 ceramic plate are 0.3 mm and 1 mm, respectively, and the other specific dimensional information of DBC substrate is indicated in Fig. 1(b). The specimen surface is cleaned with anhydrous ethanol to remove any potential oil, dust, and other contaminants, then it is placed in a vacuum oven at 90 °C to remove any residual solvent and ensure thorough drying. Subsequently, plasma treatment is applied to further clean the surface and enhance the adhesion of the encapsulant. Silicone elastomers are more suitable for the encapsulation of

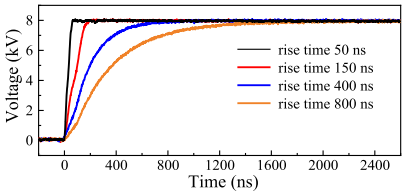

Fig. 3. Typical output waveforms of the HV square pulse generator.

HV power modules due to their better insulating properties than silicone gels. The applied encapsulant in this work is a two-component silicone elastomer (Ausbond-195, −60-200 °C of recommended operating temperature), with a mixing ratio of 10:1, and placed in a vacuum oven at 30 °C for 20 min to degas and cure. The position between two electrodes is observed with an optical microscope after the silicone elastomer is fully cured, and no obvious bubble exists, as shown in Fig. 1(b). Another 24 h of degassing are also applied after the curing to remove the possible byproducts.

B. Down-Mixing PD Detection System

The main principle of the down-mixing PD detection system is to apply a high-pass filter to suppress the EMI and extract the PD signal according to their difference in the ultrahigh frequency spectrum, and then to apply the down-mixing technology to shift to lower frequencies of the acquired signal. The system not only can effectively extract PD signals under high dV/dt square waves but also requires a lower sampling rate of the acquisition equipment due to the low-frequency band of the output signals, which is especially suitable for the detection and storage of continuous PDs under the square wave. The circuit diagram and photo of the down-mixing PD detection system are shown in Fig. 2. The ridged horn antenna (0.5–10 GHz) is applied as the PD sensor. The lower cutoff frequencies of the high-pass filters and the upper cutoff frequency of the low-pass filter are all 1 GHz. The effective frequency bands of the HF and LF amplifiers are 0.5–8 GHz and 0.1–1000 MHz, respectively, and the gain of both is 20 dB. The input and output frequency bands of the mixer are 0.75–4.2 GHz and dc-1.5 GHz, respectively. More details about the down-mixing PD detection system are described in [2].

C. Experimental Procedure

The unipolar HV square wave generator based on an HV transistor switch, as described in [2], is applied as the power supply, with an output voltage of 0 to 15 kV and 50 ns of the shortest rise time. Its circuit board design is optimized to reduce stray capacitance and parasitic inductance, and its exposed metal parts are covered with single-component silicone to avoid corona discharge and surface flashover. The typical output waveforms of the HV square wave generator are shown in Fig. 3, with no voltage overshoot at both the rising and falling edges. The electrothermal coupling-stress aging of power module packaging insulation, PD detection, and data storage experimental setup is shown in Fig. 4.

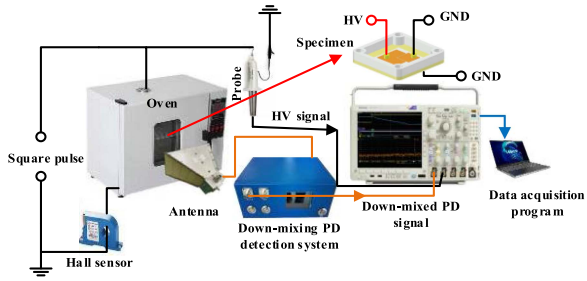

Fig. 4. Electrothermal coupling-stress aging of power module packaging insulation, PD detection, and data storage experimental setup.

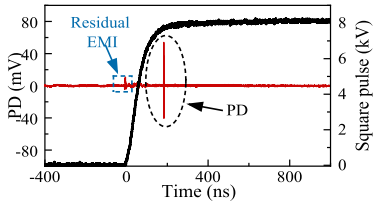

Fig. 5. Typical output PD and square pulse waveforms.

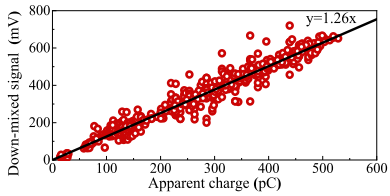

Fig. 6. Relationship between the down-mixed signal PD magnitude and apparent charge quantity.

The specimen is placed in a thermostatic oven to maintain the constant set temperature. The antenna faces the transparent glass window of the oven's door to capture the PD signal. An HV probe (Tektronix P6015a) is connected in parallel to the specimen to measure its voltage in real-time. A Hall current sensor (WCS1800) is added to monitor the current flowing through the specimen to avoid overcurrent. According to IEC 60270, the PD test standard [27], the system has been tested with no load under the square wave of 15 kV to ensure the experimental system free of PD. The L-shaped electrode of the DBC is connected to the HV and the square electrode and the baseplate are grounded, respectively. PDs only occur between the L-shaped and the square electrodes because the distance between the L-shaped electrode and the baseplate is much greater than that between it and the square electrode. The typical detected PD signal and square wave waveform are shown in Fig. 5 and it indicates that the down-mixing PD detection system provides a great signal-to-noise ratio to PD signal recognition. The approximately proportional relationship between the magnitude of electromagnetic waves generated by PDs and the amounts of apparent charges is reported [28]. The investigation of the relationship between the magnitude of the down-mixed signal and apparent charge quantity is described in [2] and it will not be elaborated further in this article. Fig. 6 shows the approximately proportional relationship between the

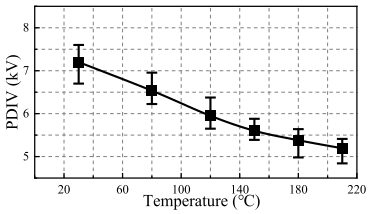

Fig. 7. PDIV of the specimen varying with temperature.

down-mixed signal magnitude and apparent charge quantity. Thus, based on that approximately proportional relationship, the down-mixed PD signal magnitude is used to characterize the PD intensity, hereafter referred to as PD magnitude.

Considering the multiconditions in the aging experiment, the description of "temperature (°C)-voltage frequency (kHz)-rise time (ns)" is adopted for the specimen (the square wave duty cycle is always fixed as 50% without additional labeling). For example, at 180 °C, applying a square wave of 5 kHz, with a rise time of 150 ns, it is described as 180-5-150. The PD inception voltage (PDIV) of the specimen needs to be measured first before aging. The parameters of the square wave for PDIV tests are set as 5 kHz of voltage frequency, 150 ns of rise time, and 50% of the duty cycle. The PDIV of each specimen is tested five times with a voltage-increasing rate of 100 V/s and the average value is regarded as the PDIV. More details about PDIV tests can be found in [2]. The tested PDIV of the specimen varying with temperature is shown in Fig. 7.

Before applying voltage, the specimen needs to be adequately heated in the oven for at least 30 min to keep a uniform temperature distribution, and an infrared thermometer is used to confirm that it reaches the set temperature. When the specimen breaks down, the aging ends and the data acquisition program stops. The duration from the start of aging to breakdown is recorded as the lifetime of the specimen. Five specimens are aged separately for each experimental condition.

III. Aging Experimental Results at Different Temperatures

For the experiments in this section, the voltage frequency and rise time of the square wave are 5 kHz and 150 ns, respectively. Experimental temperatures are set as 120, 150, 180, and 210 °C. Choosing 210 °C as the maximum temperature for the experiment considers: 1) the packaging insulation may have to be subjected to such extreme temperatures under practical working conditions and 2) the desire to explore the performance of silicone elastomer under extreme conditions. The magnitude of the square wave is set as 8 kV, which can induce continuous PDs to lead to the aging of the specimens without causing rapid breakdown.

A. PD Evolution During the Aging Process Under Different Temperatures

Generally, PD starts from the edge of the copper electrode that connects to the HV, usually at the corner position of the electrode (because the electric field is usually the highest), but sometimes

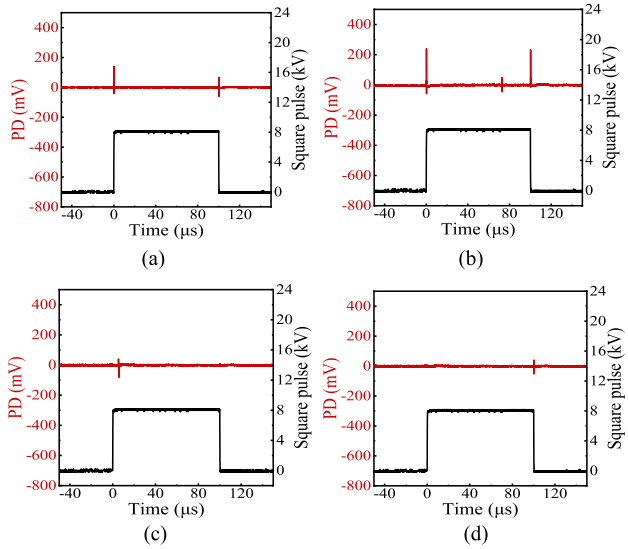

Fig. 8. Typical PD waveforms during aging. (a) Two PDs. (b) Three PDs. (c) One PD in rising edge. (d) One PD in falling edge.

there may be a start from other positions of the electrode (such as the position of the tiny tip or protrusion), and according to [17], [18], [19], [20], [21], the occurrence of the PD produces gas, and a tiny air void can form inside. The phase distribution of PD events under unipolar square wave voltage is generally related to the local transient electric field (including the applied voltage electric field and the space charge electric field) and the transient charge transport properties. Under the unipolar square wave, the mechanism of PD occurring at the rising edge and the flat part is usually attributed to local breakdown, leading to the same polarity of the discharge pulse current as the applied electric field, while PDs occurring along and after the falling edge are mostly attributed to the recombination of space charges, leading to the opposite polarity of the discharge current [12]. The space charges generated by the PD might weaken the local electric field and may also provide the initial electrons for the next PD, leading to the occurrence of phase differences in PD events. Typical PD waveforms during aging are shown in Fig. 8. Mostly, two PDs occur in one cycle, as shown in Fig. 8(a), with one at the rising edge and the other at the falling edge. The case of three PDs in one cycle can also occur sometimes, as shown in Fig. 8(b), which might indicate more than one PD location or might be because the localized electric field after the first PD still exceeds the PD onset field. In rare cases, the magnitude of the first PD during a cycle is small, resulting in fewer accumulated space charges, and then no notable PD occurs at the falling edge, as shown in Fig. 8(c). If no notable PD occurs during the rising edge or flat part of the square wave, the previously accumulated space charges may still recombine and lead to unique PD events during the falling edge, as shown in Fig. 8(d). To avoid confusion in presentation, both the first PD and second PD described below refer to the PDs that occur before the falling edge during a square wave cycle.

The magnitude and number of PDs are counted and analyzed every minute to characterize the PD evolution during aging. Considering the similarity of PD evolution processes at the

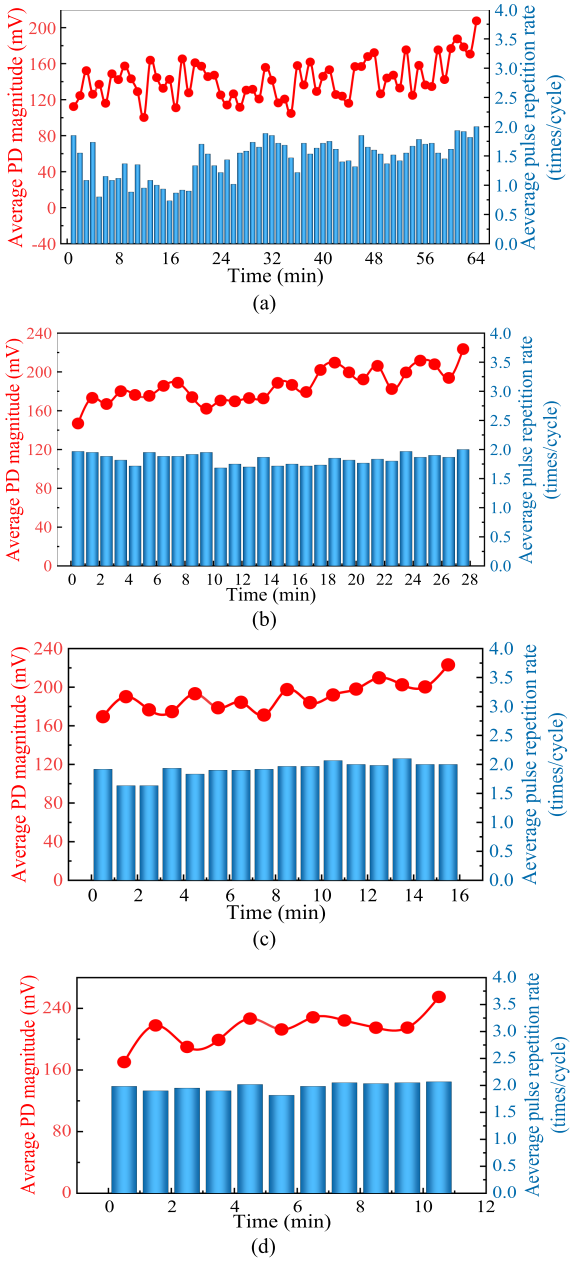

Fig. 9. Average PD magnitude and pulse repetition rate evolution of the specimen with median lifetime during aging at different temperatures. (a) 120-5-150. (b) 150-5-150. (c) 180-5-150. (d) 210-5-150.

same temperature and the limitation of space, Fig. 9 presents the average PD magnitude and average pulse repetition rate evolution during aging of the specimen with median lifetime as typical examples at different temperatures.

From Fig. 9(a)–(d), it is obvious that at 120 °C, during the initial stage of specimen aging, the PD magnitude and average pulse repetition rate are low, exhibiting a slow evolution process, while at higher temperatures, the average magnitudes of PDs usually increase at a faster rate during evolution, and the pulse repetition rates are also higher. During the aging inception stage, the PD magnitude is relatively small, while the average pulse repetition rate is usually around 2, which indicates that during the

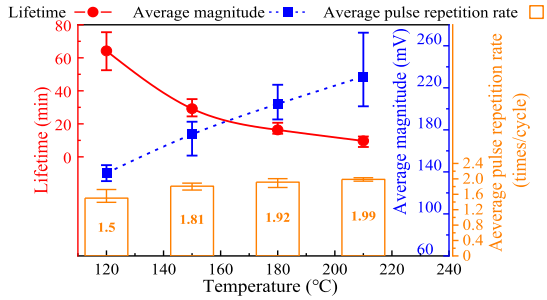

Fig. 10. Statistics of lifetimes, PD magnitudes, and pulse repetition rates under different temperatures.

aging inception stage, small PDs frequently occur. Subsequently, as aging progresses, the magnitudes of PDs do not increase monotonically over time, but show a fluctuating growth trend, while the pulse repetition rates fluctuate. This phenomenon is similar to the PD evolution of the degradation of silicone insulation containing a spherical cavity [29], which is related to the accumulation of space charges and the gas pressure in the gas cavity. Vigorous PD activity generates space charges and causes silicone elastomer to degrade and produce gas, forming the gas void. The accumulation of space charges under the unipolar square wave at both ends of the gas void reduces the localized electric field and the PD activity. Subsequently, the gas cavity volume decreases, and the space charge gradually dissipates or recombines, resulting in the enhancement of the electric field and PD activity [21]. The above cyclic process repeats, eventually leading to the aging of silicone elastomer until insulation failure occurs.

On the eve of insulation breakdown, the PD magnitude increases significantly, reaching the maximum value in the aging process, with the average magnitude increasing by more than 50% compared with the early stage of aging. The average pulse repetition rate reaches or even exceeds 2, which indicates that the PD activity is most intense right before the final breakdown occurs. The damage accumulation of PD on insulation is not only related to the PD magnitude but also the pulse repetition frequency of PDs because high-frequency PD can accelerate the degradation of insulation. Therefore, the product of the PD average magnitude and the average pulse repetition frequency per unit time can be used as a proper indicator of aging.

B. Statistics of Lifetimes, PD Magnitudes, and Pulse Repetition Rates

The lifetimes under different temperatures are plotted, as shown in Fig. 10, where the red dots indicate the average lifetime at each temperature, respectively. Fig. 10 shows that as the temperature increases, the average lifetime of power module packaging insulation decreases, and the decreasing trend becomes slower. To visualize the correlation between temperature and PD behavior, the average PD magnitude and average pulse repetition rate of all the specimens aged in this section are counted, as the blue curve and orange bars are shown in Fig. 10. The statistics in Fig. 10 show that the average PD magnitude and pulse repetition rate of the specimens during the aging tend

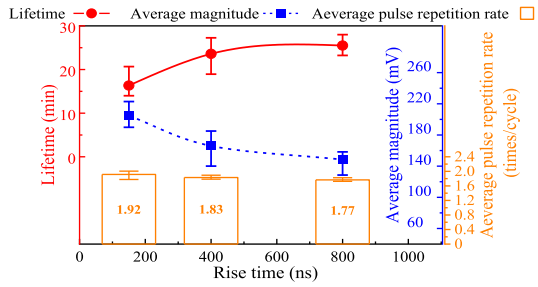

Fig. 11. Statistics of lifetimes, PD magnitudes, and pulse repetition rates under different rise times.

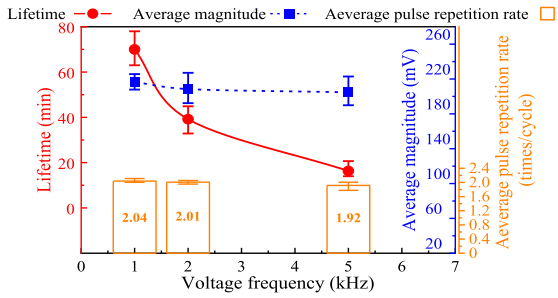

Fig. 12. Statistics of lifetimes, PD magnitudes, and pulse repetition rates under different repetition frequencies.

to increase with temperature. Moreover, for specimens at the same temperature, those with larger average PD magnitudes usually exhibit higher pulse repetition rates and shorter lifetimes. The above statistics of the experimental results describe the differences in the evolution of the PD during the aging of the power module packaging insulation at different temperatures. The impact of PDs and temperature on the lifetime will be discussed specifically in Section V.

IV. Aging Experimental Results With Different Rise Times and Voltage Frequencies

For the experiments in this section, the temperature is 180 °C, and the magnitude and duty cycle of the square wave are set as 8 kV and 50%.

A. Lifetimes and PD Behaviors With Different Rise Times

The voltage frequency of the square wave in this section is fixed as 5 kHz, and the rise times are 150, 400, and 800 ns, respectively. The variation of the average lifetimes with rise time, the average PD magnitude, and the average pulse repetition rate of all the specimens aged in this subsection during aging are shown in Fig. 11. It can be observed that at the same temperature, a longer rise time of applied square wave leads to a lower average magnitude and pulse repetition rate of PDs, in other words, weaker PD activity, tending to a longer lifetime. The correlation between PD magnitude, pulse repetition rate, and lifetime is similar to that described in Section III. Specifically, under the same experimental conditions, specimens with longer lifetimes generally exhibit relatively lower PD magnitudes and pulse repetition rates.

B. Lifetimes and PD Behaviors With Different Voltage Frequencies

The rise time of the square wave in this subsection is fixed as 150 ns, and the voltage frequencies are 1, 2, and 5 kHz, respectively. The variation of the average lifetimes of packaging insulation with voltage frequency, the average PD magnitude, and the average pulse repetition rate with different voltage frequencies are shown in Fig. 12, respectively.

As the voltage frequency decreases, the lifetime increases significantly. By comparing the lifetimes from Figs. 11 and 12, it is evident that, at the same temperature, the impact of the applied square wave voltage frequency on the lifetime of power module packaging insulation is much more significant than the rise time. This is due to that with a higher frequency applied voltage, PD occurs more frequently, leading to faster degradation of the packaging insulation. However, it should be noted that the effect of voltage frequency on lifetime is not an inversely proportional relationship. For instance, under the 1 kHz square wave, the average lifetime of the specimens is not twice that of the specimen under 2 kHz, but slightly lower. This phenomenon is attributed to the effects of voltage frequency on PD behavior. Fig. 12 exhibits that with lower frequencies, both the average magnitude and pulse repetition rate of PDs during one cycle show a slight increase. Take 1 kHz for an example, the average number of PDs per cycle exceeds 2. This also explains why the effect of the square wave voltage frequency on the packaging insulation lifetime at high temperatures with applied voltage magnitude exceeding PDIV is not inversely proportional, which is due to the more frequent PD activity during each square wave cycle at a lower frequency.

More details and mechanisms of the effects of square wave rise time and voltage frequency on the PD behavior and lifetime will be specifically analyzed in Section V.

V. Effects of the Temperature and Voltage Parameters on PD Behavior

The aging mechanisms of PD for power module packaging insulation include breaking the molecular chains, forming free radicals [17], promoting degradation [18], [19], [20], [21], and creating air voids [12], resulting in the change of the dielectric properties of the material and reduction of the insulation strength. The temperature, rise time, and frequency of the square wave affect the behavior of PD [2], which in turn affects the aging mechanism mentioned above. Therefore, this section focuses on the effect mechanisms of temperature, rise time, and frequency of the square wave on PD behavior.

A. Effects of Temperature on PD Behavior

Based on the experimental results in Section III, the increase in temperature usually leads to more intense PD activity, including the increase both in PD average magnitude and occurrence frequency, which in turn reduces the lifetime of the packaging insulation. The effects of temperature can be analyzed in the following aspects.

1) Decrease in the PDIV: From a macroscopic perspective, the decrease in PDIV can be a contributing factor to the more intense PD activity within the power module packaging insulation under high temperatures. The magnitude of the square wave is set as 8 kV, exceeding 34%, 43%, 49%, and 54% of the corresponding PDIV at 120, 150, 180, and 210 °C, respectively, according to Fig. 7, which means that higher overvoltage exists when PDs occur at a higher temperature. Higher overvoltage usually leads to higher transient localized electric field and electron generation rate [30], resulting in more severe activity of PDs. The mechanism of PDIV decreasing due to temperature increase is related to the charge transport process and variation of material properties and those will be discussed below.

2) PD Charge Transport Processes: Microscopically, the effects of temperature on the PD behaviors in power module packaging insulation can be analyzed in terms of charge transport processes. Considering the specimen structure and material properties described in Section II-A, PD always occurs in the encapsulant, which is normally polymeric material. The occurrence of PD can break the polymer chain and generate gases to form void defects. Differences in permittivity and conductivity between the gas in the void and the silicone elastomer can enhance the electric field in the void, promoting further development of PD events, and leading to hot-electron avalanches. The discharge type is usually regarded as streamer discharges, which generate sufficient magnitude of discharge pulse charges to be detected and can result in polymer aging [30]. Based on that, the PD behavior in the power module packaging insulation can be analyzed using the stochastic model [31]. When the initial gas void is formed due to PD and the localized electric field reaches or exceeds the streamer inception criterion, the PD initial electron may be provided by gas volume ionization, field emission from the void surface, photoionization in the bulk insulation material, and subsequent escape of the photoelectrons into the void [31], [32], where the surface emission is usually considered as the main source when studying PD behavior within a spherical cavity in a solid dielectric material [33], [34]. Therefore, the following analysis is based on surface emission. After the PD activity starts, the rate of electron emission from the void surface $N_{\mathrm{d}t}$, indicating the number of free electrons available to start a PD in the cavity per unit time, can be expressed as [31]

$$N_{\mathrm{d}t} \propto N_{\mathrm{d}to} \exp\left(-\frac{\Phi - \sqrt{eE/(4\pi\varepsilon)}}{kT}\right) \tag{1}$$

where $N_{\mathrm{d}to}$ is the number of electrons available for being detrapped, e is the elementary charge, E is the localized electric field inside the void, ε is the permittivity of the gas void, Φ is an effective de-trapping work function related to material, microroughness, and chemical state, and k is the Boltzmann constant. $N_{\mathrm{d}to}$ can be considered as consisting of two parts, the electrons generated by the last PD and the electrons detrapping at any loose polymer chain ends at the cavity-dielectric surface boundary [33]. For the former, PD activity is more intense at higher temperatures, providing more initial electrons for the next PD. For the latter, the number of detrapped electrons can be considered being increased by the electric field [34] and the effects of increased temperature on the material properties can lead to an elevated local electric field [35]. Thus, both are increased by higher temperatures. The last exponential term of (2) indicates that the initial free electron due to surface emission depends on the void field, temperature, and the surface work function and it can be promoted by higher temperatures [34]. Therefore, the electron emission rate from the void surface increases at higher temperatures, leading to more intense PD activity including greater PD magnitude and pulse repetition rate. Additionally, higher temperature also causes the electrons to be accelerated more effectively [36], which also results in more severe PD activity (higher magnitude and pulse repetition rate) and reduced insulation lifetime.

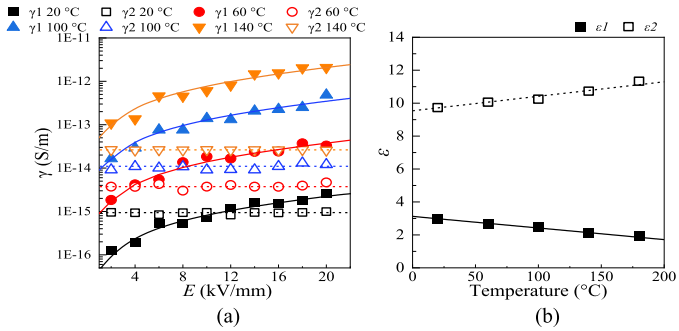

Fig. 13. Testing results of the conductivity and permittivity at different electric fields and temperatures. (a) Conductivity. (b) Permittivity.

3) Variation of Properties of the Insulation Material: In addition to the charge transport process, temperature also affects the conductivity properties of the insulation materials used for packaging insulation, which in turn changes the internal electric field distribution according to Maxwell–Wagner theory and influences the PD activity. Due to the composite insulation structure of power module packaging (including two dielectric materials: silicone elastomer and ceramics), the mismatch in permittivity and conductivity between the two dielectrics can lead to charge relaxation when the applied voltage varies. During this process, charge accumulation occurs at the interface between the two dielectric materials and affects the local electric field, particularly under dc voltage. Our previous research has proved that the conductivities and permittivity of silicone elastomer and ceramics are affected by temperature and localized electric field [35]. To better investigate the effects of the above processes and temperature variations on the local electric field within the power module packaging insulation, finite element electric field simulation considering the variations of conductivity and permittivity with temperature is applied for further analysis.

Based on the previous testing results of the conductivity and permittivity at different electric fields and temperatures, as shown in Fig. 13, and the calculation methods shown in [35], the conductivity and the permittivity of the silicone elastomer (γ_1, ε_1) and ceramics (γ_2, ε_2) can be expressed as

$$\begin{cases} \gamma_1 = 7.46 \times 10^{-7} \exp\left(-\frac{0.595e}{kT}\right) \sinh\left(1.87 \times 10^{-8} E\right) E^{0.284} \\ \gamma_2 = 9.01 \times 10^{-11} \exp\left(-\frac{0.29e}{kT}\right) \end{cases} \tag{2}$$

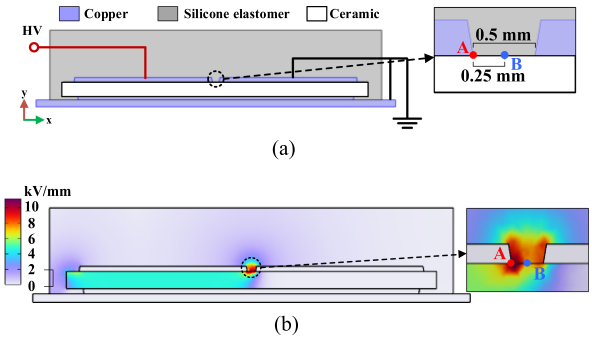

Fig. 14. Two-dimensional cross-section for power module internal electric field simulation and its typical electric field distribution. (a) Two-dimensional cross-section for power module internal electric field simulation. (b) Typical electric field distribution.

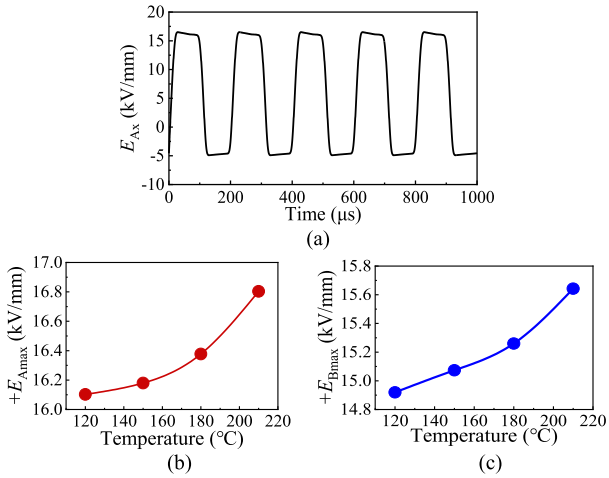

Fig. 15. Simulation results of the variation of E_{Ax} with time and maximum electric field during one cycle variation at points A and B with temperature. (a) Variation of E_{Ax} with time. (b) $E_{\max}$ at point A. (c) $E_{\max}$ at point B.

$$\begin{cases} \varepsilon_1 = -0.00705T + 5.05 \\ \varepsilon_2 = 0.00879T + 7.13 \end{cases} \tag{3}$$

where the T, E, k, and e are the same as the parameters referred to in (1). γ_2, ε_1, and ε_2 are considered temperature dependent only, while γ_1 is affected by both electric field and temperature. The simulation is based on the two-dimensional profile structure of the power module, as shown in Fig. 14(a), and its geometric parameters are consistent with the specimen. Points A and B are the triple junction and the midpoint of the two electrodes along the edge of the ceramics, respectively, which are selected as typical locations for the analysis of the electric field. The HV square wave applied to the left copper electrode is set as a magnitude of 8 kV, a frequency of 5 kHz, and a rise time of 150 ns, consistent with the experimental setup in Section III. Although the applied unipolar voltage causes the charge relaxation process and the electric field change (usually shorter than 0.1 s), the duration of the continuous square wave applied during the aging test is long enough for charges to reach the steady state. Therefore, only the results of the steady-state electric field of the simulation are analyzed. The typical electric field distribution of power module packaging insulation is shown in Fig. 14(b), where the triple junction is always the highest electric field position. In the first 50% of a square wave cycle, the electric field is usually generated by the applied voltage, while in the latter 50%, the applied voltage disappears, and the electric field is generated by the interfacial charges (not consider PDs) and its direction reverses. That process described above is shown in Fig. 15(a), taking the electric field in the x-direction at point A as an example. The simulation results of the maximum electric field during one cycle variation at points A and B with temperature are shown in Fig. 15(b) and (c). From 120 to 210 °C, the multiples of change in conductivity and permittivity for silicone elastomer and ceramic are 25.3 (γ_1, the same electric field), 3.9 (ε_1), 0.72 (γ_2), and 1.07 (ε_2), respectively. That causes an increase in the simulated electric field shown in Fig. 13(b) and (c) by about 5.0% and 5.3%, respectively. That indicates the change in conductivity and permittivity of silicone elastomer and ceramics caused by increasing temperature can lead to a higher localized electric field within the packaging insulation. It should be noted that the gas void defect formed by the PD activity is not considered in the above simulation because the composition and pressure of the gas inside the void are still unknown to calculate or test its conductivity and permittivity, making it impossible for simulation yet. Since, the gas void is usually the location of the high electric field, the change of conductivity and permittivity of the material caused by the temperature increase may lead to more severe local electric field variation than the case shown in Fig. 13, which needs to be further verified in future work.

In summary, the decrease in PDIV, the increase in PD electron generation rate, the more effective acceleration of electrons, and the elevation of the localized electric field due to changes in the conductivity properties of the insulation material are the main factors leading to more intense PD activity and lower lifetime of the power module packaging insulation at higher temperatures.

B. Effects of the Rise Time and Voltage Frequency on PD Behavior

1) Effect of the Rise Time: The experimental results in Section IV-A show that longer rise times reduce PD activity and extend the lifetime of packaging insulation. The difference in PD behaviors due to the rise time can be analyzed by the PD occurrence delay. It is widely recognized that even when the localized electric field reaches or exceeds the critical level (which can occur at a defect or a region of concentrated electric field), free electrons are also essential to trigger the PD occurrence. Consequently, there is typically a time delay between the actual occurrence of PD and the moment when the localized electric field reaches the threshold level for PD inception [31]. During that, if the magnitude of the applied voltage is higher than the PDIV as set in this article, the PD magnitude is related to the transient overvoltage. According to the estimated results in Fig. 13, the applied voltage V_{inc} of the specimen at 180 °C is about 4.7 kV. V_{PD} refers to the value of the applied voltage when the PD occurs and ΔV is the difference between V_{PD} and V_{inc}, also refers to the overvoltage. The PD delay time Δt is

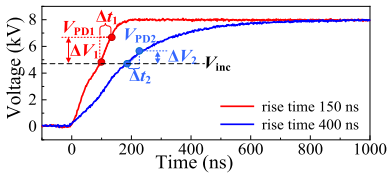

Fig. 16. Schematic of the different transient overvoltage under different rise times due to PD delay.

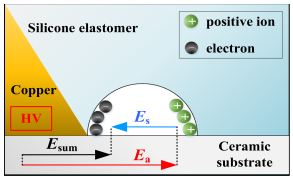

Fig. 17. Reduced localized electric field within the gas cavity due to the space charges generated by the first PD.

correlated with the magnitude of the applied voltage and other experimental conditions [31] and it would be too complicated to precisely analyze the relationship between Δt and the above factors. Therefore, for the qualitative analysis, it can be assumed that Δt_1 and Δt_2 are quite similar at the same temperature, and then the overvoltage depends on the slew rate (dV/dt). Fig. 16 illustrates that shorter rise time leads to higher overvoltage and higher transient electric field for PDs. Thus, with a shorter rise time, the PD magnitude is usually higher, resulting in the faster aging of packaging insulation.

2) Effects of the Voltage Frequency: The lower voltage frequency of the square wave leads to more intense PD activity according to the experimental results shown in Section IV-B. This phenomenon can be analyzed in terms of the process of PD occurrence. During one square wave cycle, when the localized electric field reaches the PD inception level and free electrons appear, the first PD occurs (usually near the rising edge). The space charges generated by the first PD reduce the localized electric field within the gas cavity, as shown in Fig. 17, where E_{a}, E_{s}, and E_{sum} are the applied voltage electric field, space-charge electric field, and sum electric field, respectively.

Two scenarios can be considered: 1) the localized electric field decreases below the PD inception field, then no PD occurs during the square-pulse flat region, and 2) the localized field decreases, but still exceeds the PD inception field. For scenario 1), after the falling edge, the PD occurs due to the recombination of space charges, which has been described in Section III-A. For scenario 2), the reduction of the localized electric field can lead to a longer PD delay time [31]. With a higher voltage frequency, the pulse width is shorter, and it is more likely that the applied voltage drops to zero before the initiation electron of the second PD appears. As shown in Fig. 18(a), at a wider pulse voltage, the second PD occurs, while under a narrower pulse voltage, as shown in Fig. 18(b), the applied voltage already drops to zero before the second PD occurs. Therefore, under 5 kHz, the occurrence of the second PD event in the flat region of the square wave is rare, while it is more common at 1 kHz.

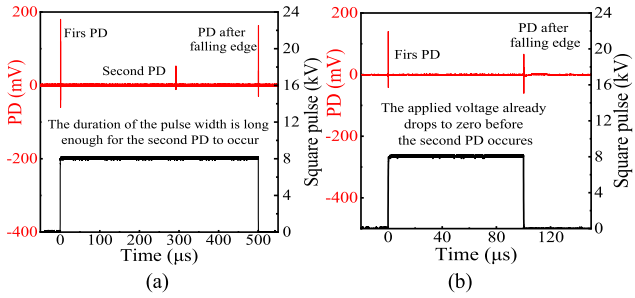

Fig. 18. Schematic diagram explaining that the second PD is less likely to occur at a shorter pulse width. (a) Wide pulse width. (b) Narrow pulse width.

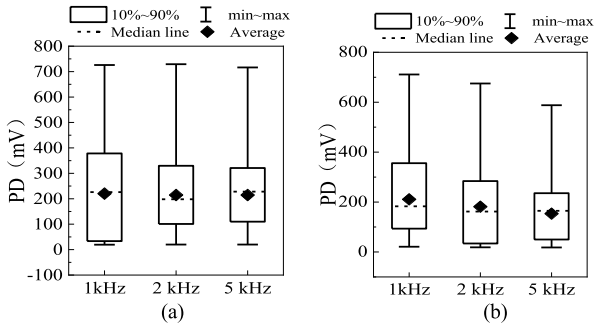

Fig. 19. Typical statistics of PD magnitudes occurring at different position during one square pulse cycle with different square pulse voltage frequency. (a) Rising edge and flat part. (b) Falling edge.

The abovementioned analysis not only explains the higher PD pulse repetition rate during a square wave cycle at lower frequencies but also the effects of frequency on the PD magnitude during aging. Due to the increase in the number of PD within the square wave cycle, more space charges are generated and lead to a stronger reverse electric field, resulting in higher magnitudes of reverse discharges during the falling edge. To validate that, the magnitudes of PDs that occur at different positions during one square wave cycle are counted, as shown in Fig. 19. It illustrates that, as the voltage frequency increases, the average magnitudes of PDs occurring at the rising edge and flat part (forward discharge) and PDs at the falling edge (reverse discharge) both tend to slightly decrease, where the decrease in the magnitude of PDs at the falling edge is more significant. At a lower frequency, the increase in the PD magnitude at the falling edge not only accelerates the degradation of the packaging insulation but also provides initial electrons for the next PD event, intensifying the PD activity at the rising edge in the next square wave cycle. Therefore, the average magnitude of PDs at the rising edge and flat part also increases slightly with decreasing frequency.

The statistics illustrated in Fig. 19 provide support for the above analysis of the more severe PD activity in a square wave cycle at a lower frequency, further explaining that under the same conditions, the lifetime of packaging insulation is not inversely proportional to the voltage frequency, but rather lower. In addition, the lifetime and PD behaviors of power module packaging insulation at low and ultrahigh voltage frequencies deserve further investigation.

VI. Lifetime Model Based on PD Damage Accumulation

Based on the experimental results and the abovementiond analysis, to better evaluate the state and failure of the power module packaging insulation under high dV/dt square wave and high-temperature coupling stress, a lifetime model considering the effects of PD aging and temperature is proposed. The existing insulation life models under electrical stress typically consider phenomena including space charge, PD, and electrical trees [30]. The lifetime models based on space charge usually consider that when the electric field exceeds a threshold, space charges penetrate the insulation bulk, high-field injection, and electron acceleration occur, gaining high energy that can break the chemical bonds of the polymer. The life model based on PD considers the damage to the chemical structure of the polymer caused by the avalanche of electrons. The idea of establishing the lifetime model in this article is to consider the PD aging factor related to discharge energy accumulation.

Under the experimental setup in this article, the end of the packaging insulation lifetime is always due to the failure of the insulation polymeric material (silicone elastomer), which is attributed to a series of irreversible chemical reactions occurring within the insulation polymeric material under multiapplied stresses degrading its electrical properties. The insulation system exhibits a stable chemical state under no applied stress. Thermal stress disrupts this state, prompting chemical reactions to proceed toward the decomposition of insulation polymeric materials, and the higher temperature would increase the chemical reaction rate. Based on the chemical reaction rate theory, the Bulk model proposed by Eyring exhibits the relation between the lifetime of insulation polymer and temperature [30], as expressed in

$$L = C_{\mathrm{E}} \left(\frac{h}{kT}\right) \exp\left(\frac{\Delta G}{kT}\right) \tag{4}$$

where L is the lifetime, h is the Planck constants, C_{E} is the model parameters depending on the material, ΔG is the Gibbs (free) energy change of the degradation process, and k and T refer to the same physical quantity as in (1). The variation of the average lifetime with temperature shown in Fig. 10 is also generally consistent with the relationship shown in (4).

The role of electrical stress on the polymer decomposition reaction is more complex. It has been shown that before the onset of PD, the applied electric field causes the free energy of the reactants to increase, resulting in a decrease in the energy barrier of the positive reaction, and accelerating the aging reaction to proceed [30]. Additionally, space charges also contribute to the aging reaction. However, once continuous PDs are initiated, the energy generated by the PD process leads to the breakage of chemical bonds and the generation of free radicals and free volumes, accelerating the aging process significantly [30]. The relationship between PD activity and packaging insulation lifetime can be established considering the damage accumulation due to PDs during aging.

The damage to insulation by PD depends mainly on the energy generated by the PD process, and when the applied voltage is constant, the energy generated by PDs is proportional to the apparent charge quantity, as expressed in

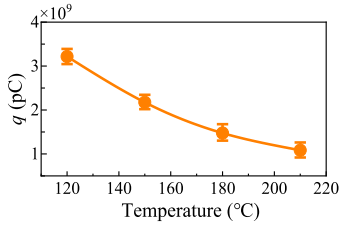

Fig. 20. Variation of Q with temperature.

$$E_{\mathrm{n}} = U \sum q_{\mathrm{i}} \tag{5}$$

where E_{n} refers to the sum of PD energy, U is the magnitude of the applied voltage, and q_{i} is the apparent charge quantity of a certain PD. Considering the correlation between the apparent charge quantity and the down-mixed signal shown in Fig. 6, the apparent charge quantity can be approximated as 1/1.26 of the down-mixed signal magnitude. The total accumulated damage due to PD during the aging process can be approximately equivalent to the sum of the apparent charge quantity, which can be estimated based on the statistics of average magnitude and pulse repetition rate, as expressed in

$$\begin{cases} Q \approx f L q_{\mathrm{a}} r_{\mathrm{a}} \\ q_{\mathrm{a}} \approx m_{\mathrm{a}}/1.26 \end{cases} \tag{6}$$

where the Q is the sum of the apparent charge quantity, q_{a}, m_{a}, and r_{a} are, respectively, the average apparent charge quantity, average magnitude, and pulse repetition rate of the PDs in each minute, L refers to the lifetime, and f is the voltage frequency of the applied square wave. Due to the design of the DBC substrate shown in Fig. 1(b), the location near the electrode corner is the location of the highest electric field, in which PD primarily occurred and the breakdown initiated. The above calculation of Q responds to the total apparent charge quantity and accumulation of PD damage in a small area near the electrode corner. The number of PD locations in this small area is subject to further determination in our future work. The statistics of Q vary with temperature shown in Fig. 20. It should be noted that the statistics of Q at 180 °C include the results at different rise times and voltage frequencies.

From Fig. 20, Q, the sum of the apparent charge quantity generated by PDs during the aging process of packaging insulation, decreases with temperature. This phenomenon may be attributed to (1) the diminished insulation performance of silicone elastomer at high temperatures, resulting in a reduced PD energy and damage accumulation requirement for aging; and (2) the promotion of material degradation reaction by high temperatures, thereby lowering the additional energy requirement. Whereas, it also indicates that at the same temperature, the value of Q varies little with the rise time and voltage frequency of the square wave. Therefore, based on this statistical result, it can be approximated that the total accumulation damage of PD during the aging of power module packaging insulation is primarily correlated with temperature. Consequently, at the same

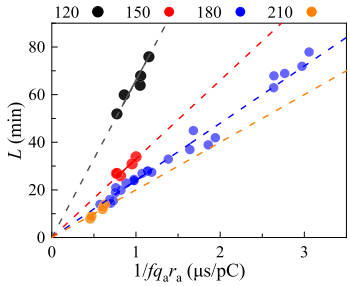

Fig. 21. Relationship between the lifetime and $(1/fm_{\mathrm{a}}r_{\mathrm{a}})$ under different temperature.

temperature, the lifetime of packaging insulation can be considered proportional to $(1/fq_{\mathrm{a}}r_{\mathrm{a}})$. The experimental results of all specimens (including those under different rise times and voltage frequencies at 180 °C) are used to verify the above inference, as shown in Fig. 21, and it illustrates that the proportionality factor for lifetime and $(1/fq_{\mathrm{a}}r_{\mathrm{a}})$ varies with temperature and the average magnitude and average pulse repetition rate of PD can be used to estimate the lifetime of power module packaging insulation.

Based on the Bulk model described in (4) and the abovementioned analysis on the accumulation damage of PD during aging, the lifetime estimation model considering temperature and PD aging factors is established in

$$L = \frac{\alpha}{Tfq_{\mathrm{a}}r_{\mathrm{a}}} \exp\left(\frac{\beta}{T}\right) \tag{7}$$

where α and β are positive coefficients related to the material property and experimental conditions. The q_{a} and r_{a} are affected by the temperature, square wave rise time, and voltage frequency. When the units of L, T, f, q_{a}, and r_{a} are, respectively, min, K, kHz, pC, and times/cycle, under the experimental setup in this article, the values of α and β are 195 (K·nC·Hz) and 1840 K according to the mathematical fit, respectively, which might be recalculated if the factors including the electric field distribution of the specimen, material properties, and the surrounding test environment are changed.

Compared with common lifetime models in [30], the model described in (7) is proposed based on the analysis of experimental results, considering the PD damage accumulation and temperature impact during the aging process. The physical and chemical mechanisms of PD-induced aging in power module packaging insulation are worth further investigation in future research.

VII. Conclusion

The aging and lifetime of power module packaging insulation due to PD under high dV/dt square wave and high-temperature coupling stresses are investigated in this article. The down-mixing PD detection system is applied to extract the PD signals. The aging experiments under different temperatures, rise times, and voltage frequencies of the square wave are carried out. Based on the mechanisms of PD and variations in material properties, the effects of temperature, rise time, and voltage frequency on the PD behavior and lifetime of power module packaging insulation are explored. The following conclusions can be drawn as follows.

1) Under unipolar high dV/dt square wave, the magnitude of PD in the packaging insulation shows a fluctuating growth trend during aging. The average magnitude and pulse repetition rate of PD reach the maximum value before breakdown failure.
2) As the temperature rises, the lifetime of the power module packaging insulation decreases, accompanied by an increase in the magnitude and pulse repetition rate of PD. The longer rise time and lower voltage frequency of the square wave tend to lead to a longer lifetime. The main influence of the longer rise time is to reduce the PD magnitude, which in turn slows down the aging process. The effect of repetition of frequency on lifetime is not inversely proportional but is usually slightly lower, which may be attributed to more intense PD activity at lower frequencies.
3) The total damage accumulation of PD during the aging of power module packaging insulation is primarily correlated with temperature. Based on that, the lifetime estimation model considering temperature and PD damage accumulation is proposed, which provides the reference for the condition evaluation of the power module.

References

[1] R. Khazaka, L. Mendizabal, D. Henry, and R. Hanna, "Survey of high-temperature reliability of power electronics packaging components," *IEEE Trans. Power Electron.*, vol. 30, no. 5, pp. 2456–2464, May 2015.
[2] Y. Ding, Y. Wang, H. Sun, and Y. Yin, "High-temperature partial discharge characteristics of power module packaging insulation under square pulse with high dV/dt based on down-mixing method," *IEEE Trans. Ind. Electron.*, vol. 70, no. 7, pp. 7334–7342, Jul. 2023.
[3] C. Bäumler, M. Hernes, J. Kowalsky, and J. Lutz, "Short circuit robustness of an aged high power IGBT-module," in *Proc. 21st Eur. Conf. Power Electron. Appl.*, Genova, Italy, 2019, pp. P.1–P.10.
[4] V. Smet et al., "Ageing and failure modes of IGBT modules in high-temperature power cycling," *IEEE Trans. Ind. Electron.*, vol. 58, no. 10, pp. 4931–4941, Oct. 2011.
[5] P. James and A. Forsyth, "Accelerated testing of IGBT power modules to determine the time to failure," in *Proc. 5th IET Int. Conf. Power Electron., Machines Drives*, Brighton, U.K., 2010, pp. 1–4.
[6] Z. Wang, "Study on easily-aging parts of solder layer in IGBT module," in *Proc. 2nd Int. Conf. Elect. Eng. Mechatron. Technol.*, Hangzhou, China, 2022, pp. 91–97.
[7] M. Bouarroudj, Z. Khatir, J.-P. Ousten, and S. Lefebvre, "Temperature-level effect on solder lifetime during thermal cycling of power modules," *IEEE Trans. Device Mater. Rel.*, vol. 8, no. 3, pp. 471–477, Sep. 2008.
[8] V. Smet, F. Forest, J.-J. Huselstein, A. Rashed, and F. Richardeau, "Evaluation of V_{ce} monitoring as a real-time method to estimate aging of bond wire-IGBT modules stressed by power cycling," *IEEE Trans. Ind. Electron.*, vol. 60, no. 7, pp. 2760–2770, Jul. 2013.
[9] E. J. De La Cruz, N. T. Yusof, W. Y. Wong, and N. I. M. Arifen, "Failure analysis of power integrated modules and its challenges," in *Proc. IEEE 23rd Int. Symp. Phys. Failure Anal. Integr. Circuits*, Singapore, 2016, pp. 395–399.
[10] H. Niu, "A review of power cycle driven fatigue, aging, and failure modes for semiconductor power modules," in *Proc. IEEE Int. Electric Machines Drives Conf.*, Miami, FL, USA, 2017, pp. 1–8.
[11] S. Diaham, Z. Valdez-Nava, T. T. Le, L. Lévêque, L. Laudebat, and T. Lebey, "Field grading composites tailored by electrophoresis—Part 3: Application to power electronics modules encapsulation," *IEEE Trans. Dielectrics Elect. Insul.*, vol. 28, no. 2, pp. 348–354, Apr. 2021.
[12] H. You, Z. We, B. Hu, Z. Zhao, R. Na, and J. Wang, "Partial discharge behaviors in power modules under square pulses with ultra-fast *dv/dt*," *IEEE Trans. Power Electron.*, vol. 36, no. 3, pp. 2611–2620, Mar. 2021.

[13] M. Ghassemi, "PD measurements, failure analysis, and control in high-power IGBT modules," *High Voltage*, vol. 3, no. 3, pp. 170–178, Mar. 2018.
[14] X. Liu et al., "Characteristics and identification of partial discharge for insulation structures in high voltage IGBT modules under positive square wave voltage," *IEEE Trans. Power Electron.*, vol. 38, no. 4, pp. 5347–5359, Apr. 2023.
[15] Y. Wang, Z. Yuan, H. Peng, Y. Ding, Y. Yin, and L. Fang, "Partial discharge testing platform for high voltage power module packaging under square wave excitation," in *Proc. IEEE Appl. Power Elect. Conf. Expo.*, 2021, pp. 1491–1495.
[16] T. Ebke, A. Khaddour, and D. Peier, "Degradation of silicone gel by partial discharges due to different defects," in *Proc. 8th Int. Conf. Dielectric Mater., Meas. Appl.*, Edinburgh, U.K., 2000, pp. 202–207.
[17] Z. Zhang, S. Zheng, S. Wu, D. Liu, A. Guan, and A. Zhong, "Analysis of electrical tree growth and partial discharge stagnation in epoxy resin," in *Proc. Int. Conf. Adv. Elect. Equip. Reliable Operation*, Beijing, China, 2021, pp. 1–4.
[18] S. Nakamura et al., "Electrical treeing in silicone gel under repetitive voltage impulses," *IEEE Trans. Dielectrics Elect. Insul.*, vol. 26, no. 6, pp. 1919–1925, Dec. 2019.
[19] S. Nakamura et al., "Effect of temperature on electrical treeing in silicone gel for power modules," in *Proc. IEEE Conf. Elect. Insul. Dielectric Phenomena*, Vancouver, BC, Canada, 2021, pp. 551–554.
[20] S. Nakamura et al., "Polarity effect on electrical treeing in silicone gel under repetitive voltage impulses," in *Proc. IEEE 3rd Int. Conf. Dielectrics*, Valencia, Spain, 2020, pp. 122–125.
[21] Z. Yan, Y. Long, K. Yang, S. Wang, Y. Zou, and J. Li, "Intrinsic self-healing characteristics of electrical tree in silicone rubber," *IEEE Trans. Dielectrics Elect. Insul.*, vol. 28, no. 3, pp. 880–887, Jun. 2021.
[22] M. Ghassemi, "Accelerated insulation aging due to fast, repetitive voltages: A review identifying challenges and future research needs," *IEEE Trans. Dielectrics Elect. Insul.*, vol. 26, no. 5, pp. 1558–1568, Oct. 2019.
[23] Y. Wang et al., "Space charge accumulation and its impact on high-voltage power module partial discharge under DC and PWM waves: Testing and modeling," *IEEE Trans. Power Electron.*, vol. 36, no. 10, pp. 11097–11108, Oct. 2021.
[24] Y. Ding, Y. Wang, and Y. Yin, "Effects of rise time and pulse width on magnitude and phase distribution of the partial discharge in power module packaging insulation under square pulse," in *Proc. IEEE 4th Int. Conf. Elect. Mater. Power Equip.*, Shanghai, China, 2023, pp. 1–4.
[25] Y. Ding, Y. Wang, M. Zhou, H. Sun, W. Li, and Y. Yin, "Partial discharge measurement of power module packaging insulation under square wave with short transition time based on SHF-down-mixing method," in *Proc. Int. Conf. Elect. Mater. Power Equip.*, 2021, pp. 1–4.
[26] D. Frey, J. L. Schanen, L. Auge, and O. Lesaint, "Electrical field investigation in high voltage power modules using finite element simulations and partial discharge measurements," in *Proc. IAS Annu. Meeting Conf. Rec. Ind. Appl. Conf.*, 2007, vol. 2, pp. 1000–1005.
[27] *High-Voltage Test Techniques-Partial Discharge Measurements*, IEC Standard 60270 Edition 3.1, IEC, Geneva, Switzerland, Nov. 2015.
[28] S. Ohtsuka, T. Teshima, S. Matsumoto, and M. Hikita, "Relationship between PD-induced electromagnetic wave measured with UHF method and charge quantity obtained by PD current waveform in model GIS," in *Proc. IEEE Conf. Elect. Insul. Dielectric Phenomena*, 2006, pp. 615–618.
[29] T. Tanmaneeprasert, P. L. Lewin, and G. Callender, "Analysis of degradation mechanisms of silicone insulation containing a spherical cavity using partial discharge detection," in *Proc. IEEE Elect. Insul. Conf.*, Baltimore, MD, USA, 2017, pp. 233–236.
[30] G. Mazzanti and G. C. Montanari, "Electrical aging and life models: The role of space charge," *IEEE Trans. Dielectrics Elect. Insul.*, vol. 12, no. 5, pp. 876–890, Oct. 2005.
[31] F. Gutfleisch and L. Niemeyer, "Measurement and simulation of PD in epoxy voids," *IEEE Trans. Dielectrics Elect. Insul.*, vol. 2, no. 5, pp. 729–743, Oct. 1995.
[32] N. Hayakawa, F. Shimizu, and H. Okubo, "Estimation of partial discharge inception voltage of magnet wires under inverter surge voltage by volume-time theory," *IEEE Trans. Dielectrics Elect. Insul.*, vol. 19, no. 2, pp. 550–557, Apr. 2012.
[33] H. Illias, G. Chen, and P. L. Lewin, "Partial discharge behavior within a spherical cavity in a solid dielectric material as a function of frequency and amplitude of the applied voltage," *IEEE Trans. Dielectrics Elect. Insul.*, vol. 18, no. 2, pp. 432–443, Apr. 2011.
[34] H. A. Illias, M. A. Tunio, H. Mokhlis, G. Chen, and A. H. A. Bakar, "Experiment and modeling of void discharges within dielectric insulation material under impulse voltage," *IEEE Trans. Dielectrics Elect. Insul.*, vol. 22, no. 4, pp. 2252–2260, Aug. 2015.
[35] M. Chen, Y. Wang, L. Fan, Y. Ding, and Y. Yin, "Temperature dependent local electric field transient analysis and measurement in high voltage power module packaging," *IEEE Trans. Dielectrics Elect. Insul.*, to be published, doi: 10.1109/TDEI.2024.3495593.
[36] C. Dervos, P. D. Bourkas, E. A. Kayafas, and I. A. Stathopulos, "Enhanced partial discharges due to temperature increase in the combined system of a solid-liquid dielectric," *IEEE Trans. Elect. Insul.*, vol. 25, no. 3, pp. 469–474, Jun. 1990.

Yi Ding received the B.S. degree in electrical engineering from Chongqing University, Chongqing, China, in 2018, and the M.S. degree in electrical engineering in 2021 from Shanghai Jiao Tong University, Shanghai, China, where he is currently working toward the Doctorate degree in electrical engineering.

His research interests include partial discharge characteristics under repetitive square wave voltage, the aging and failure mechanism of power module insulation, and charge transport characteristics in solid insulation.

Yalin Wang (Member, IEEE) received the B.Eng. degree in electrical engineering from Xi'an Jiaotong University, Xi'an, China, in 2014, and the Ph.D. degree in electrical engineering from Shanghai Jiao Tong University, Shanghai, China, in 2018.

He was a Visiting Scholar with the University of Illinois Urbana-Champaign and the University of Arkansas. He is currently an Associate Professor with Shanghai Jiao Tong University. His research interests include dielectric properties of insulation materials, power module packaging, and condition monitoring.

Meng Chen (Student Member, IEEE) received the B.S. degree in electrical engineering from Xi'an Jiaotong University, Xi'an, China, in 2017, and the M.S. degree in electrical engineering in 2020 from Shanghai Jiao Tong University, Shanghai, China, where she is currently working toward the Ph.D. degree in electrical engineering.

From 2020 to 2022, she was an Engineer with China Southern Power Grid, Guangzhou, China. Her research interests include dielectric properties of insulation, power module packaging, and its design optimization.

Lu Fan received the B.S. degree from Chongqing University, Chongqing, China, in 2017, and the Ph.D. degree from Shanghai Jiao Tong University, Shanghai, China, in 2023, all in electrical engineering.

He is currently a Postdoc with Shanghai Jiao Tong University. His research interests include charge behavior and mechanisms in polymers.

Yi Yin (Member, IEEE) was born in Jiangsu, China. He received the M.Eng. and Ph.D. degrees in electrical engineering from Xi'an Jiao Tong University, Xi'an, China, in 1997 and 2000, respectively.

He is a Professor with the Department of Electrical Engineering, School of Electronic Information and Electrical Engineering, Shanghai Jiao Tong University, Shanghai, China. His main research interests include dielectric properties of polymer composites, high-voltage technology, condition monitoring, and diagnosis.